Available online at www.sciencedirect.com
ScienceDirect
Journal of Power Sources 174 (2007) 843–846
JOURNAL OF POWER SOURCES
www.elsevier.com/locate/jpowsour

Short communication

Microscopic magnetism in lithium insertion materials of $LiNi_{1-x}Co_xO_2$ ($x = 0$, 1/4, 1/2, 3/4, and 1)

Kazuhiko Mukai [a,*], Jun Sugiyama [a], Yutaka Ikedo [a], Jess H. Brewer [b], Eduardo J. Ansaldo [c], Gerald D. Morris [c], Kingo Ariyoshi [d], Tsutomu Ohzuku [d]

[a] *Toyota Central Research and Development Laboratories, Inc., Nagakute, Aichi 480-1192, Japan*
[b] *TRIUMF, CIAR and Department of Physics and Astronomy, University of British Columbia, Vancouver, BC V6T 1Z1, Canada*
[c] *TRIUMF, 4004 Wesbrook Mall, Vancouver, BC V6T 2A3, Canada*
[d] *Department of Applied Chemistry, Graduate School of Engineering, Osaka City University (OCU), Osaka 558-8585, Japan*

Available online 28 June 2007

Abstract

The magnetic nature of lithium insertion materials of $LiNi_{1-x}Co_xO_2$ ($x = 0$, 1/4, 1/2, 3/4, and 1) were investigated by means of positive muon-spin rotation/relaxation (μ^+SR) spectroscopy combined with X-ray diffraction (XRD) analyses and susceptibility measurements. Zero field μ^+SR spectra for all the samples below 300 K were well fitted by a dynamic Kubo–Toyabe function, indicating the existence of randomly oriented magnetic moments even at 2 K, i.e., disordered state. The field distribution width Δ due to magnetic Ni^{3+} ions decreases exponentially with increasing x, suggesting that the Co substitution is likely to simply dilute Ni moments. This also supports that cobalt and nickel ions are homogeneously distributed in a solid matrix even in a muon-scale (microscopically), which is consistent with the results of macroscopic measurements.

Keywords: Lithium-ion battery; Muon-spin rotation/relaxation (μ^+SR); Magnetism; Lithium nickel cobalt oxides

1. Introduction

Muon-spin rotation/relation (μ^+SR) spectroscopy is very sensitive to local magnetic environment and one of the powerful techniques to detect both static and dynamic internal magnetic fields from 0.1 Oe to 100 kOe caused by nuclear and electronic origin [1]. According to macroscopic magnetic measurements, $LiCoO_2$ is paramagnet down to 5 K [2,3], because the Co^{3+} ions are in the low-spin state with $S = 0$ ($t_{2g}^6 e_g^0$). However, μ^+SR detects a long-range antiferromagnetic order below 30 K probably due to charge separation of Co^{3+} ions at low temperatures ($2Co^{3+} \rightarrow Co^{2+} + Co^{4+}$) [4]. The Ni^{3+} ions in $LiNiO_2$, which is isostructural to $LiCoO_2$, are also in the low-spin state with of $S = \frac{1}{2}$ ($t_{2g}^6 e_g^1$) [5]. Although the magnetism of $LiNiO_2$ samples are strongly affected by Ni ions at the Li layer, an antiferromagnetic transition below ~10 K is usually observed by susceptibility (χ) measurements [6,7]. The recent μ^+SR experiment however showed the absence of long-range order even at 2 K but a spin-glass-like fast fluctuation below 10 K for $Li_{0.98}Ni_{1.02}O_2$ [8]. The μ^+SR experiments hence provide microscopic information on a ground state of $LiCoO_2$ and $LiNiO_2$.

In this paper, we report microscopic magnetism of lithium insertion materials of $LiNi_{1-x}Co_xO_2$ ($0 \le x \le 1$) by μ^+SR combined with the macroscopic measurements such as, X-ray diffraction (XRD) analyses and χ measurements.

2. Experimental

Powder samples of $LiNi_{1-x}Co_xO_2$ ($x = 0$, 1/4, 1/2, 3/4, and 1) were prepared by a solid-state reaction technique [9–12] using reagent grade $LiNO_3$ (or $LiOH^{\bullet}H_2O$), $NiCO_3$, and $CoCO_3$. Reaction mixtures were pressed into a pellet (23 mm diameter and *ca*. 5 mm thickness) and heated at 650 °C in an oxygen flow for 15 h. The pre-calcined pellet was then ground and pressed into a pellet again, and was subsequently fired at 750 °C in oxygen flow for 15 h. For $LiCoO_2$, the reaction mixture was heated at 900 °C in air for 15 h. The final products were characterized by a powder XRD (RINT-2200, Rigaku Co. Ltd., Japan) and an induction coupled plasma (ICP) atomic emission spectral (AES) analyses, and χ measurements using a superconducting

* Corresponding author.
E-mail address: e1089@mosk.tytlabs.co.jp (K. Mukai).

0378-7753/$ – see front matter © 2007 Elsevier B.V. All rights reserved.
doi:10.1016/j.jpowsour.2007.06.105

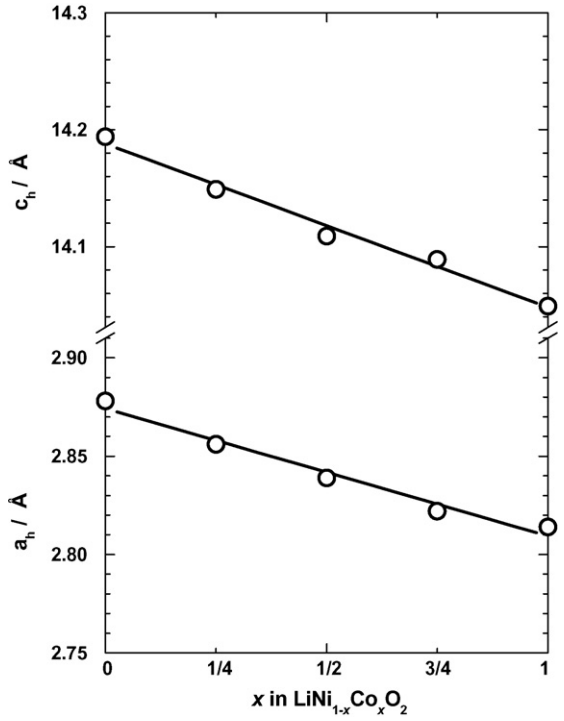

Fig. 1. Lattice constant of a_h- and c_h-axes as a function of x for $LiNi_{1-x}Co_xO_2$.

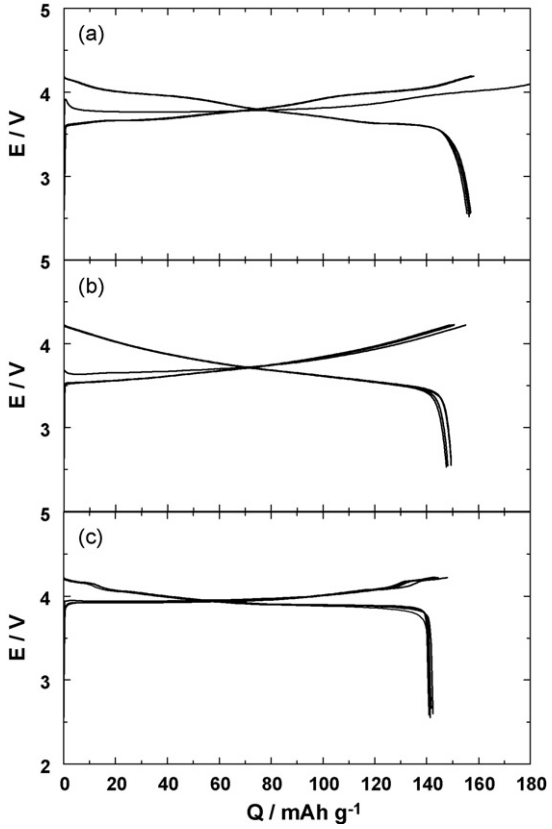

Fig. 2. Charge and discharge curves of (a) $Li/LiNiO_2$, (b) $Li/LiNi_{1/2}Co_{1/2}O_2$ and (c) $Li/LiCoO_2$ cells operated at 0.17 mA cm^{-2} in the voltage range between 2.5 and 4.2 V at 25 °C.

quantum interference device (SQUID) magnetometer (MPMS, Quantum Design). The XRD data were obtained by using an X-ray diffractometer with Cu Kα radiation. χ were measured in the temperature range between 5 and 400 K under magnetic field $H = 10$ kOe.

In preparing the electrodes, polyvinylidene fluoride (PVdF) dissolved in *N*-methyl-2-pyrrolidone (NMP) solution was used as a binder. The black viscous slurry consisting of 88 wt% active material, 6 wt% acetylene black, and 6 wt% PVdF was cast on an aluminum foil with blade. NMP was evaporated at 120 °C for 30 min, and finally the electrodes (1.5 cm × 2.0 cm) were dried under vacuum at 150 °C for 12 h. For electrochemical tests, the counter electrode was prepared by pressing lithium metal onto a stainless steel substrate. Two sheets of porous polypropylene membrane (Celgard 2500) were used as a separator. Electrolyte used was 1 M $LiPF_6$ dissolved in ethylene carbonate (EC)/dimethyl carbonate (DMC) (3/7, v/v) solution.

The μ^+SR experiments were performed on M20 surface muon beam line at TRIUMF in Vancouver, Canada. One gram of $LiNi_{1-x}Co_xO_2$ powder were pressed into a pellet (17 mm diameter and *ca.* 1 mm thickness) and placed in the sample holder of cryostat. The experimental setup and technique were described in elsewhere [13].

3. Results and discussion

The prepared samples were identified as a layered structure with a space group of $R\bar{3}\,m$, in which transition metal and lithium ions are located at 3a and 3b sites, respectively, in a cubic close-packed oxygen array. Fig. 1 shows the change in lattice constants as a function of x for $LiNi_{1-x}Co_xO_2$. The length of *a*- and *c*-axes in the hexagonal unit-cell was calculated by a least-squared method using at least 13 diffraction lines. Both a_h and c_h decrease linearly with increasing x, indicating that $LiNi_{1-x}Co_xO_2$ is a solid solution of $LiCoO_2$ and $LiNiO_2$.

Fig. 2 shows the charge and discharge (C/D) curves of (a) $Li/LiNiO_2$, (b) $Li/LiNi_{1/2}Co_{1/2}O_2$ and (c) $Li/LiCoO_2$ cells operated at a rate of 0.17 mA cm^{-2} in the voltage range between 2.5 and 4.2 V at 25 °C. The C/D curve for $LiNiO_2$ exhibits the operating voltages above 3.5 V with a couple of plateaus at *ca.* 3.6 and 4.0 V. The rechargeable capacity (Q_r) in the voltage range between 2.5 and 4.2 V is *ca.* 160 mAh g^{-1}. According to the ratio of the integrated XRD peaks $I(0\,0\,3)/I(1\,0\,4)$ and the ICP-AES, the amount of Ni ions at the Li sites for the $LiNiO_2$ sample is below 0.04, that is, $z \leq 0.04$ in $(Li_{1-z}Ni_z)_{3b}[Ni_{1-z}]_{3a}O_2$. As seen in Fig. 2(b), $LiNi_{1/2}Co_{1/2}O_2$ shows the lowest operating voltage among the four samples with $Q_r = 150$ mAh g^{-1}. The continuous change in the slope of the C/D curve, i.e. the absence of plateaus, is a characteristic feature of $LiNi_{1/2}Co_{1/2}O_2$. $LiCoO_2$ shows the highest operating voltage, while the $Q_r \sim 140$ mAh g^{-1}. The operating voltage between 0 and 70 mAh g^{-1} seems to be almost constant (∼3.9 V). The structural and electrochemical properties for the present samples are thus consistent with the previous results [9–12].

Fig. 3 shows temperature (T) dependence of (a) χ and (b) χ^{-1}. χ was measured in field-cooling (FC) mode with $H = 10$ kOe. The $\chi(T)$ curves for $LiNi_{1-x}Co_xO_2$ show a Curie–Weiss paramagnetic behavior down to *ca.* 100 K except for $LiCoO_2$. A

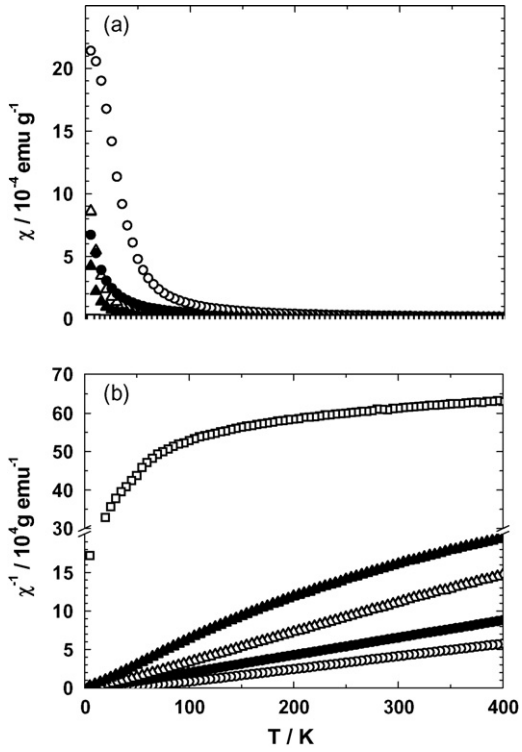

Fig. 3. Magnetic susceptibility (a) χ and (b) χ^{-1} for $LiNi_{1-x}Co_xO_2$; $x=0$ ($LiNiO_2$, open circles), $x=1/4$ (closed circles), $x=1/2$ (open triangles), $x=3/4$ (closed triangles), and $x=1$ ($LiCoO_2$, open squares). χ was measured in field-cooling (FC) mode with $H=10$ kOe.

rapid increase in χ with decreasing T is observed below 100 K for $LiNiO_2$ and below 50 K for $LiNi_{1-x}Co_xO_2$ ($x=1/4$, 1/2, and 3/4). For the paramagnetic state, the Curie–Weiss law in the general form is written as

$$\chi = \frac{N\mu_{\text{eff}}^2}{3k_{\text{B}}(T-\Theta_{\text{p}})} + \chi_0, \quad (1)$$

where N is the number of Ni and Co ions per gram, μ_{eff} the effective magnetic moment of Ni and Co ions, k_{B} the Boltzmann's constant, T the absolute T, Θ_{p} the paramagnetic Curie T, and χ_0 is the T-independent susceptibility. Using Eq. (1) in the T range between 200 and 400 K, we obtain the values of μ_{eff} for $LiNi_{1-x}Co_xO_2$ ($x=0$, 1/4, 1/2, and 3/4), as shown in Fig. 4. The value of μ_{eff} decreases monotonously with increasing x for $LiNi_{1-x}Co_xO_2$ as expected. The dotted line represents the theoretical μ_{eff} using the low-spin state configuration for $Co^{3+}(S=0)$ and $Ni^{3+}(S=\frac{1}{2})$ ions with $g=2$. The discrepancy between the experiment and the theoretical calculation (26% for $LiNiO_2$) is probably due to an enhancement of the g-factor caused by a local Jahn-Teller distortion of NiO_6-octahedra in $LiNi_{1-x}Co_xO_2$ [14].

Fig. 5 shows the zero-field (ZF)-μ^+SR spectra in the time domain (a) below 10 μs and (b) below 0.1 μs at 2 K. The ZF-μ^+SR spectrum for $LiNiO_2$ exhibits a very fast relaxation mainly observed below 0.02 μs, as reported for $Li_{0.98}Ni_{1.02}O_2$ [7] in which the explicit formula of actual $LiNiO_2$ sample is represented by $(Li^+_{1-z}Ni^{2+}_z)_{3b}[Ni^{2+}_zNi^{3+}_{1-z}]_{3a}O_2$. The Ni^{2+} ions at the Li sites is also known to enhance a ferromagnetic interaction probably due to the ferrimagnetic cluster formed by the intralayer Ni^{2+}–O–Ni^{3+} coupling [15]. However, since the fast relaxation is not observed for the sample with $z=0.07$ (not shown), the fast relaxation is considered to be an intrinsic feature of $LiNiO_2$. Note that the relaxation rate suppressed by the Co substitution of Ni as seen in the ZF-μ^+SR spectrum for $LiNi_{1/2}Co_{1/2}O_2$ (Fig. 5(b)). In order to examine the relaxation rate, the ZF-μ^+SR spectra were fitted with a combination

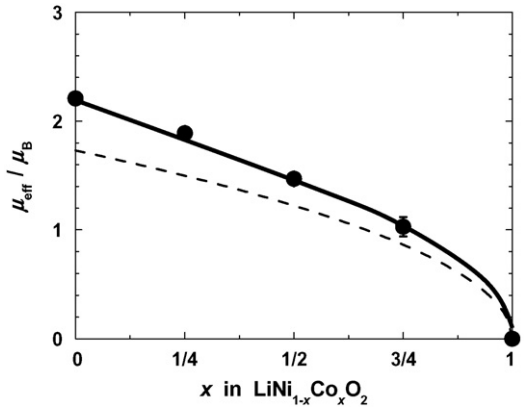

Fig. 4. Effective magnetic moments μ_{eff} as a function of x for $LiNi_{1-x}Co_xO_2$. The dotted line is the theoretical value for $LiNi_{1-x}Co_xO_2$ using the assumption that Ni^{3+} and Co^{3+} are in the low-spin state with $S=\frac{1}{2}$ and $g=2$, and $S=0$, respectively.

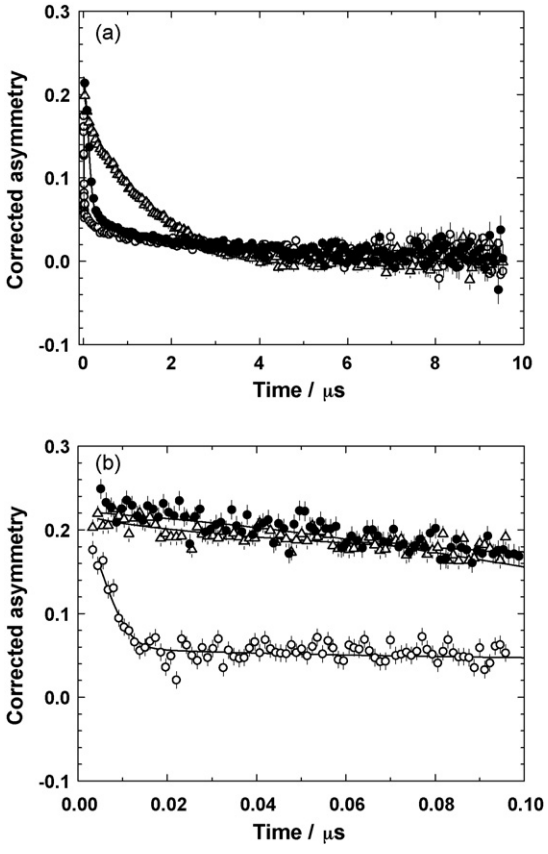

Fig. 5. ZF-μ^+SR time spectra in different time domains: (a) 0–10 μs and (b) 0–0.1 μs, for $LiNiO_2$ (open circles), $LiNi_{1/2}Co_{1/2}O_2$ (closed circles), and $LiCoO_2$ (open triangles). Fitting result by using Eq. (2) for each curve is given by solid curves.

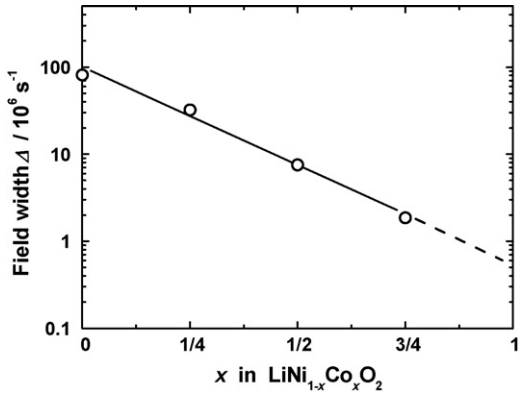

Fig. 6. The static width of the local field Δ as a function of x for $LiNi_{1-x}Co_xO_2$. A linear relation between log Δ and x is observed.

of a dynamic Kubo–Toyabe signal [16] and an exponentially relaxation signal.

$$A_0 P(t) = A_{KT} G^{DGKT}(t, \Delta, \nu) + A_S \exp(-\lambda_S t), \quad (2)$$

where A_0 is the empirical maximum muon decay asymmetry, A_{KT} and A_S are the asymmetries of a dynamic Kubo–Toyabe component due to magnetic Ni^{3+} ions and a slowly relaxing component originated from nuclear magnetism of ^7Li and ^{59}Co, λ_S the slow relaxation rate, Δ the static width of the local fields at the disordered sites, and ν is the field fluctuation rate ("hopping" rate). When $\nu = 0$, $G^{DGKT}(t, \Delta, \nu)$ is the static Gaussian Kubo–Toyabe function $G^{KT}(t, \Delta)$ given by

$$G^{KT}(t, \Delta) = \frac{1}{3} + \frac{2}{3}(1 - \Delta^2 t^2) \exp\left(-\frac{\Delta^2 t^2}{2}\right). \quad (3)$$

Fig. 6 shows the field distribution width Δ as a function of x for $LiNi_{1-x}Co_xO_2$. The data were obtained by fitting ZF-μ^+SR time spectra with Eq. (2). A linear relation is observed in the log (Δ) versus x curve. In other words, Δ decreases exponentially with increasing x, suggesting a significant role of Ni^{3+} moments on Δ. This also strongly indicates that the distribution of cations is microscopically homogeneous in $LiNi_{1-x}Co_xO_2$, that is, the solid solution of $LiNiO_2$ and $LiCoO_2$ in a microscopic scale.

In summary, we applied the μ^+SR technique to clarify the microscopic magnetism on lithium insertion materials of $LiNi_{1-x}Co_xO_2$ and found the drastic decrease in the static width of the local fields (Δ) with x. Although the origin of the x dependence of Δ is currently unclear, we expect that further μ^+SR experiments on electrochemically oxidized $Li_{1-y}CoO_2$ and $Li_{1-y}NiO_2$ provide a clear insight on the microscopic nature of lithium insertion materials in relation to electrochemical reactivity.

Acknowledgements

We wish to thank Mr. T. Ichikawa and Mr. S. Kohno of OCU in preparing and examining $LiNi_{1-x}Co_xO_2$. We appreciate Mr. Y. Kondo of Toyota Central R&D Labs. Inc. for ICP-AES measurements. We also thank Dr. B. Hitti, Dr. D.J. Arseneau, and Dr. S.R. Kreitzman of TRIUMF for their help on μ^+SR experiments. This work was partially (JHB) supported at University of British Columbia by Canadian Institute for Advanced Research, the Natural Sciences and Engineering Research Council of Canada and the National Research Council of Canada.

References

[1] J.H. Brewer, Encyclopedia Appl. Phys. 11 (1994) 23–53, and references cited therein.
[2] S. Kikkawa, S. Miyazaki, M. Koizumi, J. Solid State Chem. 62 (1986) 35–39.
[3] D. Carlier, I. Sadoune, L. Croguennec, M. Ménétrier, E. Surad, C. Delmas, Solid State Ionics 144 (2001) 263–276.
[4] J. Sugiyama, H. Nozaki, J.H. Brewer, E.J. Ansaldo, G.D. Morris, C. Delmas, Phys. Rev. B 72 (2005) 144424.
[5] J.B. Goodenough, D.G. Wickham, W.J. Croft, J. Phys. Chem. Solids 5 (1958) 107–116.
[6] J.N. Reimers, J.R. Dahn, J.E. Greedan, C.V. Stager, G. Liu, I. Davidson, U. von Sacken, J. Solid State Chem. 102 (1993) 542–552.
[7] A. Rougier, C. Delmas, G. Chouteau, J. Phys. Chem. Solids 57 (1996) 1101–1103.
[8] T. Chatterji, W. Henggeler, C. Delmas, J. Phys. Condens. Matter 17 (2005) 1341–1350.
[9] T. Ohzuku, A. Ueda, M. Nagayama, J. Electrochem. Soc. 140 (1993) 1862–1870.
[10] A. Ueda, T. Ohzuku, J. Electrochem. Soc. 141 (1994) 2972–2976.
[11] T. Ohzuku, A. Ueda, M. Nagayama, Y. Iwakoshi, H. Komori, Electrochim. Acta 38 (1993) 1159–1167.
[12] T. Ohzuku, Y. Makimura, Res. Chem. Intermed. 32 (2006) 507–521.
[13] G.M. Kalvius, D.R. Noakes, O. Hartmann, in: K.A. Gschneidner Jr., et al. (Eds.), Handbook on the Physics and Chemistry of Rare Earths, vol. 32, North-Holland, Amsterdam, 2001, pp. 55–451, and references cited therein.
[14] H. Yoshida, Y. Muraoka, T. Sörgel, M. Jansen, Z. Hiroi, Phys. Rev. B 73 (2006), 020408 (R).
[15] E. Chappel, M.D. Nunez-Regueiro, S. de Brion, G. Chouteau, V. Bianchi, D. Caurant, N. Baffier, Phys. Rev. B 66 (2002) 132412.
[16] R.S. Hayano, Y.J. Uemura, J. Imazato, N. Nishida, T. Yamazaki, R. Kubo, Phys. Rev. B 20 (1979) 850–859.